Earth Syst. Dynam. Discuss., 5, 747–778, 2014
www.earth-syst-dynam-discuss.net/5/747/2014/
doi:10.5194/esdd-5-747-2014

Earth System Dynamics Discussions
Open Access

Path dependence of climate and carbon cycle response over a broad range of cumulative carbon emissions

T. Herrington and K. Zickfeld

Department of Geography, Simon Fraser University, Burnaby, Canada

Received: 23 May 2014 – Accepted: 23 May 2014 – Published: 17 June 2014

Correspondence to: K. Zickfeld (kzickfel@sfu.ca)

Published by Copernicus Publications on behalf of the European Geosciences Union.

Abstract

Recent studies have demonstrated the proportional relationship between global warming and cumulative carbon emissions, yet the robustness of this relationship has not been tested over a broad range of cumulative emissions and emission rates. This study explores the path dependence of the climate and carbon cycle response using an Earth System model of intermediate complexity forced with 24 idealized emissions scenarios across five cumulative emission groups (1275–5275 GtC) with varying rates of emission. We find the century-scale climate and carbon cycle response after cessation of emissions to be approximately independent of emission pathway for all cumulative emission levels considered. The ratio of global mean temperature change to cumulative emissions – referred to as the transient climate response to cumulative emissions (TCRE) – is found to be constant for cumulative emissions lower than ~ 1500 GtC, but to decline with higher cumulative emissions. The TCRE is also found to decrease with increasing emission rate. The response of Arctic sea ice is found to be approximately proportional to cumulative emissions, while the response of the Atlantic meridional overturning circulation (AMOC) does not scale linearly with cumulative emissions, as its peak response is strongly dependent on emission rate. Ocean carbon uptake weakens with increasing cumulative emissions, while land carbon uptake displays non-monotonic behavior, increasing up to a cumulative emission threshold of ~ 2000 GtC and then declining.

1 Introduction

Recent studies with coupled climate-carbon cycle models have shown that global mean temperature change is independent of emission pathway and approximately proportional to cumulative CO_2 emissions (Allen et al., 2009; Matthews et al., 2009; Zickfeld et al., 2009, 2012; Gillett et al., 2013). Results have also suggested that global mean temperature remains approximately constant for centuries to millennia after CO_2

ESDD
5, 747–778, 2014

emissions cease (Plattner et al., 2008; Eby et al., 2009; Solomon et al., 2009; Frölicher and Joos, 2010; Gillett et al., 2011; Zickfeld et al., 2013).

These studies can be characterized as using the "cumulative emissions framework", which relates the instantaneous or century-scale response of global mean temperature to the cumulative CO_2 emissions over a certain period of time. The ratio of global mean temperature change to cumulative CO_2 emissions, referred to as the Transient Climate Response to Carbon Emissions (TCRE), is a measure of both the carbon cycle response to CO_2 emissions and the physical climate response to atmospheric CO_2 increase, and has been suggested as a useful benchmark for model intercomparison (Matthews et al., 2009; Gillett et al., 2013). The cumulative emissions framework is also useful to climate policy discussions for it enables to express temperature targets, such as the 2 °C target adopted by many countries and international organizations, in terms of a carbon emission "budget" (England et al., 2009; Meinshausen et al., 2009; Zickfeld et al., 2009; Messner et al., 2010).

Several studies explored the robustness of the proportional relationship between the century-scale and instantaneous global mean temperature change and cumulative emissions. Studies with both Earth System Models of Intermediate Complexity (EMICs) (Eby et al., 2009; Zickfeld et al., 2009) and complex Earth System Models (ESMs) (Zickfeld et al., 2012; Nohara et al., 2013) demonstrated that the *century-scale* temperature response after cessation of emissions is independent of emissions pathway. Zickfeld et al. (2012), using the Canadian Earth system model (CanESM), showed that the path independence holds also for a range of other climate variables (atmospheric CO_2 concentration, precipitation, sea ice cover, Atlantic meridional overturning circulation). Nohara et al. (2013) obtained similar results with the Community Earth System Model (CESM), except for the response of the Atlantic meridional overturning circulation, which was found to exhibit path dependence in a cumulative CO_2 emission overshoot scenario.

A range of studies also explored the robustness of the proportional relationship between the *instantaneous* global mean temperature change and cumulative

ESDD
5, 747–778, 2014

emissions by evaluating the constancy of the TCRE. Matthews et al. (2009), using results from C^{4}MIP simulations found the TCRE to be constant up to cumulative emissions of about 2000 GtC. This result was confirmed by Gillett et al. (2013), who used results from the CMIP5 1 % CO_2 increase experiment. Both studies tested the constancy of the TCRE for one emisson scenario only. Zickfeld et al. (2012) explored the TCRE for a set of scenarios with varying emission rates, and found it to be approximately constant across scenarios. Krasting et al. (2014), on the other hand, using a range of scenarios with constant CO_2 emission rates (2–25 GtC yr^{-1}), found the TCRE to vary with emission rate. They found the TCRE to be highest at low and high emission rates, and lowest at present-day emission rates (5–10 GtC yr^{-1}).

Previous studies exploring the proportional relationship between climate change and cumulative carbon emissions either focused on a single emission scenario (Matthews et al., 2009; Gillett et al., 2013) or on emission scenarios with cumulative CO_2 emissions of up to about 2500 GtC (Zickfeld et al., 2012; Nohara et al., 2013). Here we use the University of Victoria Earth System Climate Model (UVic ESCM) to explore the transient climate and carbon cycle response to emisson pathways spanning a broad range of cumulative CO_2 emissions and CO_2 emission rates. To this scope, we design a set of CO_2 emission scenarios pertaining to five cumulative emission groups (1275 GtC, 2275 GtC, 3275 GtC, 4275 GtC, and 5275 GtC). Each cumulative emission group includes a variety of peak-and-decline scenarios, an "overshoot" scenario entailing negative CO_2 emissions, and a "pulse" scenario with instantaneous CO_2 release.

The paper begins with an overview of the UVic ESCM, followed by a description of the emission scenarios designed for the purpose of this study. Section 3 is divided into three main components. First, the transient response of the physical climate system is explored. Next, an analysis of the relationship between physical climate variables and cumulative emissions is presented, followed by an exploration of the carbon cycle response. Finally, the paper ends with a summary of key findings and conclusions.

ESDD
5, 747–778, 2014

2 Methods

2.1 Model description

The study utilized the UVic ESCM version 2.9, which includes an ocean general circulation model coupled to a sea ice model and energy-moisture balance model of the atmosphere, and land and ocean carbon cycle models. The ocean model consists of a primitive 3-dimensional, 19-layer ocean general circulation model with isopycnal mixing and a Gent and McWilliams (1990) parameterization of the effect of eddy-induced tracer transport. Diapycnal mixing is modeled using a horizontally constant profile of diffusivity with values on the order of $0.3 \times 10^{-4}\,m^2\,s^{-1}$ in the pycnocline (Weaver et al., 2001; Eby et al., 2009). Coupled to the ocean model are a dynamic-thermodynamic sea ice model, and a thermodynamic energy-moisture balance model of the atmosphere with dynamical feedbacks (Weaver et al., 2001). Land surface and terrestrial vegetation dynamics are modeled using a simplified version of the Hadley Centre Met Office surface exchange scheme (MOSES) coupled to the Top-Down Representation of Interactive Foliage and Flora Including Dynamic vegetation model (TRIFFID) (Meissner et al., 2003). Ocean carbon is represented via an Ocean Carbon Cycle Model Intercomparison Project (OCMIP) type inorganic ocean carbon cycle model and a nutrient-phytoplankton-zooplankton-detritus marine ecosystem model (Schmittner et al., 2005). Sediment processes are represented using an oxic-only model of sediment respiration (Archer, 1996). Model coverage is global with a zonal resolution of 3.6° and meridional resolution of 1.8° (Weaver et al., 2001).

2.2 Model simulations

2.2.1 Historical simulation

The historical simulation was started from the model's pre-industrial (year 1800) control configuration (with a CO_2 concentration of 284 ppm), and integrated to the year 2008

ESDD
5, 747–778, 2014

using the observed CO_2 fossil fuel (Boden et al., 2012) and land use change (LUC) emissions (Houghton, 2008), along with radiative forcing from non-CO_2 greenhouse gas (CH_4, N_2O, and halocarbons), sulphate aerosols and surface albedo changes associated with LUC. Natural forcings, including solar variations (due to changes in solar luminosity and orbital configuration) and volcanic eruptions, were applied using the observed forcing until 2000, and then kept at constant 2000-levels over the rest of the simulation. Between 1800 and 2008, the cumulative CO_2 fossil fuel and LUC emissions were 347 GtC and 210 GtC, respectively, resulting in a year 2008 CO_2 concentration of 382 ppm.

2.2.2 Future emission pathways

Twenty four idealized emission scenarios across five cumulative emission groups (1275 GtC, 2275 GtC, 3275 GtC, 4275 GtC, and 5275 GtC) were designed (Table 1). These scenarios include both fossil fuel and land use change emission, and span a variety of peak and decline scenarios with varying emission rates, as well as cumulative emission "overshoot" scenarios with negative emissions and instantaneous pulse scenarios (Fig. 1). The emission scenarios were designed by setting a target peak emission rate and a target year of emission cessation, and ensuring total cumulative emissions (from 1800 onwards) fit into one of the five aforementioned cumulative emission groups. The emission scenarios include a cumulative 275 GtC of LUC emissions as well as a cumulative 1000–5000 GtC of fossil fuel emissions. LUC emissions follow the historical LUC emissions to 2008 and then decline linearly, reaching zero by 2100, while all fossil fuel emissions end by 2400 (Table 1).

The fossil fuel and LUC emission scenarios were used to force future simulations spanning the period 2008–3000. Simulations were run with the same forcings as over the historical period. The radiative forcing from land use change (albedo effect), solar, orbital, and volcanic forcings were kept constant at year 2000-levels, while sulphate and non-CO_2 GHGs followed the Special Report on Emission Scenarios (SRES) A2 scenario until 2010, and were held constant at year 2010 levels thereafter.

ESDD
5, 747–778, 2014

3 Results and discussion

3.1 Physical climate changes

3.1.1 Atmospheric CO_2 concentration

Peak atmospheric CO_2 concentration varies from 575 ppm in the 1275 GtC VFAST to 2521 ppm in the 5275 GtC PULSE scenario (Fig. 2). Scenarios with higher emission rates yield higher peak CO_2 concentrations; a function of land and ocean carbon sinks being unable to keep up with faster emission rates (Eby et al., 2009; Zickfeld et al., 2012).

Though the short-term CO_2 concentration varies by scenario, the CO_2 concentration begins to converge after emission cessation for scenarios with the same cumulative emissions, and the long-term CO_2 concentration (by the year 3000) is independent of the emissions rate; a characteristic which is common to all five cumulative emission groups.

Initially, the increased atmospheric CO_2 concentration promotes increased photosynthesis and water use efficiency in plants ("CO_2 fertilization"; Wullschleger et al., 2002) allowing for rapid uptake of CO_2 by the land. However, as emissions cease and CO_2 declines while surface air temperature remains elevated, the land becomes a weak net carbon source, leaving the much slower ocean sink to take up excess CO_2 (Fig. 9).

3.1.2 Surface air temperature

The short-term response of global mean surface air temperature (SAT) is dependent on emission scenario, with scenarios entailing higher maximum emission rates yielding a faster initial increase in temperature (Fig. 3). After emissions cease, however, temperature curves within a cumulative emissions group converge towards a common value, suggesting that the long-term (year 3000) global mean temperature response

ESDD
5, 747–778, 2014

is pathway independent and only dependent on the overall cumulative emissions (Eby et al., 2009; Zickfeld et al., 2009; Zickfeld, 2012). Remarkably, despite substantially higher peak CO_2 concentrations in the OVST and PULSE scenarios, the peak temperature is nearly identical to that of the other scenarios in the same cumulative emissions group, suggesting that the peak temperature anomaly is also approximately independent of the emission rate (Allen et al., 2009). The year 3000 global mean temperature anomaly (relative to the year 1800) ranges between 2.4 °C for the 1275 GtC scenarios and 8.9 °C for the 5275 GtC scenarios. The spatial pattern of temperature change at the year 3000 is shown in Fig. 4 for one select scenario from each cumulative emission group.

The temperature anomaly after cessation of emissions is found to remain approximately constant, with lower cumulative emission groups (1275 and 2275 GtC) showing a slight temperature decline after peaking, and higher cumulative emission groups (3275–5275 GtC) showing a slight temperature increase. The near-constancy of global mean temperature after cessation of emissions is in agreement with earlier modeling studies (Matthews et al., 2008; Plattner et al., 2008; Eby et al., 2009; Solomon et al., 2009; Frölicher and Joos, 2010; Gillett et al., 2011; Zickfeld et al., 2012) and is thought to arise because the cooling effect associated with declining CO_2 is compensated by reduced ocean heat uptake (Eby et al., 2009).

We also found the *regional* temperature response at the year 3000 to be approximately independent of emission pathway. For instance, the maximum temperature difference between the 5275 GtC PULSE and SLOW scenarios at the year 3000 is ~ 0.2 °C over Central Asia (Fig. 4f).

3.1.3 Thermosteric sea level

Global thermosteric sea level rise, defined as the rise in sea level due to thermal expansion of the ocean, is much slower to react to the increased radiative forcing than surface temperature. The year 3000 thermosteric sea level rise (relative to 1800) ranges between 0.9 m for the 1275 GtC scenarios to 2.7 m for the 5275 GtC PULSE

ESDD
5, 747–778, 2014

scenario (Fig. 5). Though thermosteric sea level rise shows sensitivity to emission rate in the short term (with faster emission rates yielding a faster initial sea level rise), the curves slowly converge over the course of the simulation, such that even in the 5275 GtC simulations, there is only a 0.08 m difference between the SLOW and PULSE simulations by the year 3000. The small difference is due to the millennial response timescale of the deep ocean to changes in radiative forcing.

The finding of path independence of thermosteric sea level rise over century timescales is similar to the findings of other studies (Zickfeld et al., 2012; Bouttes et al., 2013), and is a function of the proportionality of thermosteric sea level rise to the time integrated radiative forcing (Zickfeld et al., 2012; Bouttes et al., 2013).

3.1.4 Arctic sea ice

September Arctic sea ice disappears completely in the 3275–5275 GtC scenarios, while it reaches a minimum of about 0.25×10^6 to 0.28×10^6 km^2 ($\sim$ 5.5 to 6 % of the year 2000 value) in the 2275 GtC scenarios, and 2.6×10^6 km^2 in the 1275 GtC scenarios ($\sim$ 58 % of the year 2000 value) (Fig. 6).

The rate of sea ice decline is path dependent, and a function of the CO_2 emission rate. Emission scenarios with a higher maximum CO_2 emission rate display the fastest declines. The minimum sea ice extent, on the other hand, is independent of emission pathway.

Our simulations suggest that there is a threshold cumulative emissions level at which the modeled climate is no longer able to support year-round sea ice cover. Using the definition of an ice-free Arctic adopted by the IPCC's Fourth Assessment Report (AR4), in which a minimum ice extent of $\leq 1.0 \times 10^6$ km is considered ice free (Solomon et al., 2007), this threshold lies between 1275 and 2275 GtC.

The UVic model fails to capture the current observed trends of rapid ice loss in the last decade (Comiso, 2012), a problem that plagues many climate models (Stroeve et al., 2007). The inability of the model to simulate the observed decline in sea ice

ESDD
5, 747–778, 2014

suggests that the threshold cumulative emission levels for an ice-free Arctic in the summer may be lower than indicated by this study.

3.1.5 Atlantic Meridional Overturning Circulation

The modeled Atlantic Meridional Overturning Circulation (AMOC) index (defined as the maximum of the overturning streamfunction) is 20.7 Sv in the year 2000, which is in relatively good agreement with observations (~ 12 to ~ 30 Sv over the past decade) (Send et al., 2011). The simulated AMOC is quite robust for even in the 5275 GtC scenarios the AMOC index never falls below 13 Sv or ~ 59 % of the preindustrial value before recovering (Fig. 7). Recovery of the AMOC occurs after temperatures at high latitudes begin to stabilize and freshwater fluxes into the North Atlantic begin to stabilize or slow, allowing the overturning circulation to export some of the excess freshwater from the region.

The transient response of the AMOC is dependent on emission pathway – with pathways displaying higher emission rates producing a faster decline and a deeper minimum. The long-term (year 3000) response of the AMOC, however, is path independent, although the curves are slower to converge at higher cumulative emission levels.

Rahmstorf (2000) suggested that the AMOC may be subject to hysteresis or multiple stable states – where the overturning circulation can be on or off, or associated with different locations of deep water formation. The robustness of the AMOC in the UVic model, even at extremely high CO_2 concentrations (such as in the case of the 5275 GtC scenarios), either suggests that multiple stability states are not present in the UVic ESCM, or that the forcing is below the critical threshold required to induce a state transition. The model, however, does not include all potential feedbacks on the AMOC, including those associated with melt-water fluxes from Greenland, so it is possible that the AMOC decline is underestimated by the model.

ESDD
5, 747–778, 2014

3.2 Relationship between physical climate response and cumulative emissions

3.2.1 Surface air temperature

Consistent with previous studies (Matthews et al., 2009; Zickfeld et al., 2012; Gillett et al., 2013), we find an approximately linear relationship between the modeled instantaneous surface air temperature change (ΔT) and total cumulative emissions (E_c) (Fig. 9a). We use linear regression to calculate the ratio of ΔT to E_c, referred to as the Transient Climate Response to Cumulative Emissions (TCRE) (Gillett et al., 2013). We obtain values of 1.9–2.0 °C per trillion tons of carbon (TtC) for the 1275 GtC scenarios, 1.8–1.9 °C TtC^{-1} for the 2275 GtC scenarios, 1.6–1.7 °C TtC^{-1} for the 3275 GtC scenarios, 1.5–1.6 °C TtC^{-1} for the 4275 GtC scenarios, and 1.3–1.5 °C TtC^{-1} for the 5275 GtC scenarios. These results indicate that the TCRE decreases with increasing cumulative emissions. Furthermore, the slight variation of the TCRE within cumulative emission groups suggests that the TCRE is sensitive to the emission rate, with the TCRE decreasing with increasing rates of emission. The TCRE calculated at the time of doubling of the pre-industrial CO_2 concentration ranges between 1.7 °C TtC^{-1} (for the 5275 GtC OVST scenario) and 1.9 °C TtC^{-1} (for the 1275 GtC scenarios).

The spread in the regression-based TCRE values of 0.6 °C TtC^{-1} for the scenarios examined in this study compares to a spread of 1.1 °C TtC^{-1} for C^{4}MIP models (1.0–2.1 °C TtC^{-1}; Matthews et al., 2009) and 1.6 °C TtC^{-1} for CMIP5 models (0.8–2.4 °C TtC^{-1}; Gillett et al., 2013). This indicates that the sensitivity of the TCRE to emission pathway is substantial, albeit smaller than the sensitivity to structural differences in the suite of C^{4}MIP and CMIP5 models.

The tendency for the TCRE to decrease at higher cumulative emissions was noted in earlier studies for cumulative emissions in excess of 2000 GtC (Matthews et al., 2009) and 3000 GtC (Gillett et al., 2013). In a study with the GFDL model using scenarios with a range of linear emission increase rates, Krasting et al. (2014) found the TCRE to increase with increasing emission rates (for emission rates of 5–25 GtC yr^{-1}), which is the opposite tendency from that found in this study.

ESDD
5, 747–778, 2014

The linear relationship between ΔT and E_c depends on the cancellation of the saturation of carbon sinks with increasing E_c and increasing rate of emissions (which results in a larger airborne fraction; see Fig. 9) and the logarithmic dependence of radiative forcing on atmospheric CO_2 (which results in a smaller increase in radiative forcing per unit CO_2 increase at higher CO_2 levels). The decrease in TCRE with increasing E_c and higher emission rates suggests that the effect of saturation of the radiative forcing dominates over the effect of a higher airborne fraction of CO_2 at higher cumulative emissions and emission rates in the UVic ESCM.

3.2.2 Peak temperature

The relationship between peak surface air temperature and cumulative emissions (Allen et al., 2009) shows a slight deviation from linearity as cumulative emissions increase (Fig. 8b). Within cumulative emissions groups, the peak temperature is approximately independent of the emissions rate, with the exception of the 1275 and 2275 GtC OVST scenarios. The peak at higher cumulative emissions in the 1275 and 2275 GtC OVST scenarios is the result of the fact that in these scenarios, peak temperature occurs during the overshoot phase, whereas in the higher cumulative emission groups peak temperature occurs near the end of the millennium.

3.2.3 Atlantic meridional overturning circulation

The peak response of the AMOC is dependent on the emission pathway, with scenarios entailing the highest emission rates yielding the largest declines in overturning circulation. The minimum overturning, unlike peak surface air temperature, does not display a linear relationship with cumulative emissions (Fig. 8c). The minimum overturning shows strong path dependence with higher emission rates yielding a deeper AMOC minimum. We also find that the minimum overturning decreases with increasing cumulative emissions.

ESDD
5, 747–778, 2014

The instantaneous AMOC response does not scale well with cumulative emissions either (not shown), consistent with the result from earlier studies (Zickfeld et al., 2012; Nohara et al., 2013).

3.2.4 Arctic sea ice

Similar to the findings of Zickfeld et al. (2012), the response of September Arctic sea ice (ΔI), which is closely correlated to Northern Hemisphere temperature change, scales approximately linearly with cumulative emissions. There generally is, however, a steeper change in sea ice per unit change in cumulative emissions ($\Delta I / E_c$) for scenarios with lower rates of emission and lower cumulative emissions (Fig. 8d). This likely arises from the fact that the TCRE declines with increasing cumulative emissions and increasing emission rates.

3.3 Changes in the carbon cycle

3.3.1 Atmospheric carbon burden

Until emissions cease, the airborne fraction (defined as the ratio of atmospheric carbon burden changes to cumulative emissions) varies substantially across emission pathways within the same cumulative emission group (Fig. 9a and b), and is largest for emission pathways with the highest emission rates. For the 5275 GtC scenarios, the maximum airborne fraction varies between 72 % for the SLOW scenario and 90 % for the PULSE scenario.

The airborne fraction also varies substantially between cumulative emissions groups, increasing with increasing cumulative emissions (Plattner et al., 2008; Zickfeld et al., 2013). For the lower cumulative emission groups (1275 and 2275 GtC), less than half of the emitted CO_2 remains airborne by the year 3000, while for higher cumulative emission groups, more than half of the emitted CO_2 still resides in the atmosphere.

ESDD
5, 747–778, 2014

The year 3000 airborne fraction is 29 % for the 1275 GtC scenarios and 63 % for the 5275 GtC scenarios.

3.3.2 Ocean carbon uptake

The ocean takes up a large proportion of the cumulative emissions (Fig. 9e and f). Until emission cessation, ocean carbon uptake is relatively rapid, with > 50 % of the emissions taken up before emissions cease. Uptake slows substantially afterwards, primarily due to declining atmospheric CO_2 levels.

The ocean uptake fraction decreases significantly with increasing cumulative emissions. By the year 3000, ocean carbon uptake amounts to 56 % of cumulative emissions in the 1275 GtC scenarios, and 35 % in the 5275 GtC scenarios. The decrease in ocean uptake fraction with increasing cumulative emissions is due to a decrease in the CO_2 buffering capacity of the ocean and stronger climate-carbon cycle feedbacks at higher cumulative emissions (Plattner et al., 2008; Zickfeld et al., 2013).

Ocean carbon uptake across the different emission scenarios is slower to converge than their atmospheric CO_2 counterparts – a function of the ocean's sluggish response to changes in atmospheric forcing. By the year 3000, however, the differences across scenarios within a cumulative emission group are < 0.5 %, even for the 5275 GtC scenarios.

3.3.3 Land carbon uptake

The terrestrial biosphere takes up a relatively small fraction of the cumulative carbon emissions (3–15 % of the total by the year 3000), but displays interesting dynamics (Fig. 9c and d).

Initially, global land carbon exhibits a rapid increase, driven primarily by the CO_2 fertilization effect. Despite much higher peak atmospheric CO_2 levels, peak land carbon uptake is very similar in the 2275–5275 GtC scenarios, indicating that there is a limit to

ESDD
5, 747–778, 2014

the amount of carbon which can be taken up by the terrestrial biosphere in the UVic model.

After 2100 or so (earlier in the PULSE scenarios), global land carbon declines in most scenarios. The timing and magnitude of the decline is strongly dependent on the emission scenario (both in terms of total cumulative emissions and emission rate). For the 1275 GtC scenarios, the decline results in losses of about 70–130 GtC of land carbon between 2100 and 3000. In the 2275 GtC scenarios, land carbon declines are much more modest, ranging between about 20 and 30 GtC, as carbon losses in tropical regions are approximately balanced by gains in high latitude regions.

To some degree in the 3375 GtC scenarios, but noticeably more so in the 4275 and 5275 GtC scenarios, "roller-coaster" type behaviour is evident in land carbon, where the initial CO_2 fertilization driven increase of land carbon is followed by a decline, before undergoing a slow recovery towards the end of the simulation. This decline in land carbon after the peak is a result of carbon losses in the Tropics (Fig. 10a) associated with temperature-driven mortality of tropical broadleaf forest (in tropical South America, SE Asia, and tropical Africa), and replacement by C4-grass and shrub. The increase in land carbon following the "dip" is driven by expansion of boreal needleleaf forest, as it displaces shrub and C3-grass tundra at high latitudes. Land carbon continues to decline in the Tropics over this time period, but is dominated by land carbon gain at high northern latitudes (Fig. 10b).

Land carbon uptake does not show a monotonic response with increasing cumulative emissions, owing to temperature related declines at higher cumulative emissions (3275–5275 GtC) outweighing any CO_2 fertilization driven increase. Despite having the highest atmospheric CO_2 concentration, the 5275 GtC scenarios feature the smallest absolute and fractional land carbon uptake, while the 4275 GtC scenarios have the third highest absolute uptake and the second smallest fractional uptake. Absolute uptake values increase between the 1275 GtC and 2275 GtC scenarios, before declining, while fractional uptake values are highest in the 1275 GtC scenarios. This suggests

ESDD
5, 747–778, 2014

that threshold behaviour may be occurring in global land carbon, driven by strong temperature related losses at higher levels of cumulative emissions (3275–5275 GtC).

Slight path dependence is evident in the 5275 GtC scenarios, with the PULSE scenario showing slightly lower land carbon uptake than the other scenarios (Fig. 9c). Throughout the model integration, the PULSE scenarios shows less land carbon uptake at high latitudes and more uptake in the Tropics than its counterparts, but by the end of the model integration, the land carbon difference in the PULSE scenario originates from central Asia, where C3 grass is replaced by needleleaf and shrub (not shown), which is not the case in the other scenarios.

Compared to other EMICs, land carbon uptake in the UVic ESCM is quite weak (Plattner et al., 2008; Zickfeld et al., 2013). Land carbon uptale in the UVic ESCM exhibits high sensitivities to both CO_2 and temperature (Eby et al., 2013), which implies a strong CO_2 fertilization, effect, but also strong climate-carbon cycle feedbacks. Unlike previous studies, which found the land uptake fraction to remain relatively constant or decrease slightly with increasing cumulative emissions (Plattner et al., 2008; Zickfeld et al., 2013), we find the land uptake fraction to decrease substantially with increasing cumulative emissions. These previous studies, however, explored a narrower range of cumulative emissions (up to about 3800 GtC in Zickfeld et al., 2013).

4 Summary and conclusions

This study explores the path dependence of the climate and carbon cycle response under CO_2 scenarios spanning a broad range of cumulative emissions and emission rates. We use the UVic Earth System Model of intermediate complexity, which is forced with 24 CO_2 emission scenarios across five cumulative emission groups (1275 GtC, 2275 GtC, 3275 GtC, 4275 GtC, and 5275 GtC). Each cumulative emission group includes a variety of peak and decline scenarios with differing emission rates, an overshoot scenario, and an instantaneous pulse scenario.

ESDD
5, 747–778, 2014

Our results indicate that the century-scale global mean temperature response after cessation of CO_2 emissions is independent of emission pathway and proportional to cumulative emissions, consistent with the findings of previous studies (Eby et al., 2009; Zickfeld et al., 2009, 2012; Nohara et al., 2013).

The ratio of global mean temperature change to cumulative emissions – referred to as the transient climate response to cumulative emissions (TCRE) – is found to be constant for cumulative emissions lower than ~ 1500 GtC, but to decline with higher cumulative emissions. The TCRE is also found to decrease with increasing peak emission rate, in contrast to the results from another study (Krasting et al., 2014).

The century-scale thermosteric sea level rise is also found to be approximately independent of emission pathway. Small differences in sea level rise between scenarios within the same cumulative emisson group at the end of the simulation arise from the sluggish response of the ocean to radiative forcing.

Similarly to global mean temperature and thermosteric sea level rise we find the long-term response of Arctic September sea ice cover to be independent of emission pathway and determined only by cumulative emissions. The long-term sea ice cover declines with increasing cumulative emissions, with a critical cumulative emission level for the loss of year-round Arctic sea ice found to be between 1275 and 2275 GtC. Changes in Arctic September sea ice cover also show an approximately proportional relationship with cumulative emissions, with the change in sea ice cover per unit change in cumulative emissions differing slightly across scenarios and cumulative emission groups.

The peak response of the Atlantic meridional overturning circulation (AMOC) is found to be path dependent, with pathways featuring higher emission rates yielding the largest AMOC decline. Eventually, however, the AMOC responses converge, and there is little difference in the year 3000 AMOC strength across scenarios within a cumulative emission group. At no point does the AMOC shutdown in any of the 24 scenarios, suggesting that either the AMOC in the UVic ESCM does not exhibit multiple stable states, or that the critical transition point was not reached.

ESDD
5, 747–778, 2014

Similarly to the physical climate variables, the century-scale carbon cycle response after cessation of emissions is found to be approximately independent of emission pathway. Small differences in year 3000 ocean carbon uptake between scenarios at high cumulative emission levels arise from the slow response of the ocean to changes in atmospheric CO_2 and temperature. We also find a small difference in year 3000 land carbon uptake between scenarios at high cumulative emissions (5275 GtC) due to hysteresis in regional land cover changes.

The year 3000 land carbon uptake exhibits a non-monotonic response to cumulative CO_2 emissions, with land carbon uptake increasing for cumulative emissions up to 2275 GtC and then decreasing. This indicates that for cumulative emissions greater than 2275 GtC, land carbon gains associated with the CO_2 fertilization effect are more than offset by warming related losses. Expressed as a fraction of cumulative emissions, land carbon uptake at year 3000 is largest for the 1275 GtC scenarios (15 %) and declines with increasing cumulative emissions, to just 3 % for the 5275 GtC scenarios.

Ocean carbon uptake at year 3000 increases in absolute terms with increasing cumulative emissions, as a function of increasing atmospheric CO_2 levels at higher cumulative emissions. The fraction of cumulative CO_2 emissions taken up by the ocean at the year 3000 decreases with increasing cumulative emissions, from 56 % in the 1275 GtC scenarios to 35 % in the 5275 GtC scenarios. As a result of reduced fractional land and carbon uptake with increasing cumulative emissions, the year 3000 airborne fraction of CO_2 increases with increasing cumulative emissions, from 29 % in the 1275 GtC scenarios to 63 % in the 5275 GtC scenarios.

In summary, this study shows that the long-term climate and carbon cycle response is approximately independent of emission pathway over a broad range of cumulative emissions. This study also confirms the approximately proportional relationship between global warming and cumulative carbon emissions. The TCRE deviates from constancy for cumulative emissions greater than ~ 1500 GtC and is sensitive to the rate of emissions, but these path dependencies are a smaller source of uncertainty in the TCRE than inter-model differences.

ESDD
5, 747–778, 2014

Author Contribution

K. Zickfeld conceived the study, T. Herrington and K. Zickfeld. designed the model experiments, T. Herrington performed the model simulations and analyzed the data, T. Herrington and K. Zickfeld interpreted the data and wrote the manuscript.

Acknowledgements. K. Zickfeld acknowledges support from the National Science and Engineering Research Council (NSERC) CREATE and Discovery Grant Programs.

References

Allen, M., Frame, D., Huntingford, C., Jones, C. D., Lowe, J. A., Meinshausen, M., and Meinshausen, N.: Greenhouse-gas emission targets for limiting global warming to 2˚C, Nature, 458, 1163–1166, 2009.

Archer, D.: A data-driven model of the global calcite lysocline, Global Biogeochem. Cy., 10, 511–526, 1996.

Boden, T. A., Marland, G., and Andres, R. J.: Carbon Dioxide Information Analysis Center, Oak Ridge National Laboratory, US Department of Energy, Oak Ridge, Tenn., USA, available at: http://cdiac.ornl.gov/trends/emis/tre_glob_2009.html (last access: 30 September 2012), 2012.

Bouttes, N., Gregory, J. M., and Lowe, J. A.: The reversibility of sea level rise, J. Climate, 26, 2502–2513, 2013.

Comiso, J. C.: Large decadal decline of the Arctic multiyear ice cover, J. Climate, 25, 1176–1193, 2012.

Eby, M., Zickfeld, K., Montenegro, A., Archer, D., Meissner, K., and Weaver, A.: Lifetime of anthropogenic climate change: millennial time scales of potential CO_2 and surface temperature perturbations, J. Climate, 22, 2501–2511, 2009.

England, M. H., Gupta, A. S., and Pitman, A. J.: Constraining future greenhouse gas emissions by a cumulative target, P. Natl. Acad. Sci. USA, 106, 16539–16540, 2009.

Frölicher, T. L. and Joos, F.: Reversible and irreversible impacts of greenhouse gas emissions in multi-century projections with the NCAR global coupled carbon cycle-climate model, Clim. Dynam., 35, 1439–1459, 2010.

ESDD
5, 747–778, 2014

Gent, P. R. and Mcwilliams, J. C.: Isopycnal mixing in ocean circulation models, J. Phys. Oceanogr., 20, 150–155, 1990.
Gillett, N. P., Arora, V. K., Zickfeld, K., Marshall, S. J., and Merryfield, W. J.: Ongoing climate change following a complete cessation of carbon dioxide emissions, Nat. Geosci., 4, 83–87, 2011.
Gillett, N. P., Arora, V. K., Matthews, H. D., and Allen, M. R.: Constraining the ratio of global warming to cumulative CO_2 emissions using CMIP5 simulations, J. Climate, 26, 6844–6858, 2013.
Houghton, R. A.: Carbon Dioxide Information Analysis Center, Oak Ridge National Laboratory, US Department of Energy, Oak Ridge, Tenn., USA, available at: http://cdiac.ornl.gov/trends/landuse/houghton/houghton.html (last access: 30 September 2012), 2008.
Krasting, J. P., Dunne, J. P., Shevliakova, E., and Stoufer, R. J.: Trajectory sensitivity of the transient climate response to cumulative carbon emissions, Geophys. Res. Lett., 41, 2520–2527, 2014.
Matthews, H. D. and Caldeira, K.: Stabilizing climate requires near-zero emissions, Geophys. Res. Lett., 35, L04705, doi:10.1029/2007GL032388, 2008.
Matthews, H. D., Gillett, N. P., Stott, P. A., and Zickfeld, K.: The proportionality of global warming to cumulative carbon emissions, Nature, 459, 829–832, 2009.
Meinshausen, M., N., Meinshausen, Hare, W., Raper, S. C. B., Frieler, K., Knutti, R., Frame, D. J., and Allen, M. R.: Greenhouse-gas emission targets for limiting global warming to 2 °C, Nature, 458, 1158–1162, 2009.
Meissner, K., Weaver, A., Matthews, H., and Cox, P.: The role of land surface dynamics in glacial inception: a study with the UVic Earth System Model, Clim. Dynam., 21, 515–537, 2003.
Messner, D., Schellnhuber, J., Rahmstorf, S., and Klingenfeld, D.: The budget approach: a framework for a global transformation toward a low-carbon economy, Journal of Renewable and Sustainable Energy, 2, 1–14, 2010.
Nohara, D., Yoshida, Y., Misumi, K., and Ohba, M.: Dependency of climate change and carbon cycle on CO_2 emission pathways, Environ. Res. Lett., 8, 014047, doi:10.1088/1748-9326/8/1/014047, 2013.
Plattner, G., Knutti, R., Joos, F., Stocker, T., Von Bloh, W., Brovkin, V., Cameron, D., Driesschaert, E., Dutkiewicz, S., and Eby, M.: Long-term climate commitments projected with climate-carbon cycle models, J. Climate, 21, 2721–2751, 2008.

ESDD
5, 747–778, 2014

Rahmstorf, S.: The thermohaline ocean circulation: a system with dangerous thresholds?, Climatic Change, 46, 247–256, 2000.
Schmittner, A., Oschlies, A., Giraud, X., Eby, M., and Simmons, H.: A global model of the marine ecosystem for long-term simulations: sensitivity to ocean mixing, buoyancy forcing, particle sinking, and dissolved organic matter cycling, Global Biogeochem. Cy., 19, GB3004, doi:10.1029/2004GB002283, 2005.
Send, U., Lankhorst, M., and Kanzow, T.: Observation of decadal change in the Atlantic meridional overturning circulation using, 10 years of continuous transport data, Geophys. Res. Lett., 38, L24606, doi:10.1029/2011GL049801, 2011.
Solomon, S., Qin, D., and Manning, M.: Climate Change 2007: The Physical Science Basis, Working Group I Contribution to the Fourth Assessment Report of the Intergovernmental Panel on Climate Change, Cambridge University Press, Cambridge, UK, 2007.
Solomon, S., Plattner, G., Knutti, R., and Friedlingstein, P.: Irreversible climate change due to carbon dioxide emissions, P. Natl. Acad. Sci. USA, 106, 1704–1709, 2009.
Stroeve, J., Holland, M. M., Meier, W., Scambos, T., and Serreze, M.: Arctic sea ice decline: faster than forecast, Geophys. Res. Lett., 34, L09501, doi:10.1029/2007GL029703, 2007.
Weaver, A. J., Eby, M., Wiebe, E. C., Bitz, C. M., Duffy, P. B., Ewen, T. L., Fanning, A. F., Holland, M. M., MacFadyen, A., and Matthews, H. D.: The UVic Earth System Climate Model: model description, climatology, and applications to past, present and future climates, Atmos. Ocean, 39, 361–428, 2001.
Wullschleger, S., Tschaplinski, T., and Norby, R.: Plant water relations at elevated CO_2 – implications for water-limited environments, Plant, Cell Environ., 25, 319–331, 2002.
Zickfeld, K., Eby, M., Matthews, H. D., and Weaver, A. J.: Setting cumulative emissions targets to reduce the risk of dangerous climate change, P. Natl. Acad. Sci. USA, 106, 16129–16134, 2009.
Zickfeld, K., Arora, V. K., and Gillett, N. P.: Is the climate response to CO_2 emissions path dependent?, Geophys. Res. Lett., 39, L05703, doi:10.1029/2011GL050205, 2012.
Zickfeld, K., Eby, M., Alexander, K., et al.: Long-term climate change commitment and reversibility: an EMIC intercomparison, J. Climate, 26, 5782–5809, 2013.

ESDD
5, 747–778, 2014

Table 1. The 24 emission scenarios and their characteristics. Emissions include both fossil fuel and land-use change emissions.

Cumulative Emission Group	Scenario	Maximum Emission Rate (GtC yr^{-1})	Year of Emission Cessation
1275 GtC	FAST	14.1	2100
	VFAST	17.4	2100
	OVST	16.9	2100
	PULSE	376.7	2010
2275 GtC	FAST	17.1	2100
	MEDIUM	14.9	2100
	SLOW	11.5	2250
	OVST	18.7	2100
	PULSE	883.5	2010
3275 GtC	FAST	19.1	2200
	MEDIUM	14.7	2250
	SLOW	12.9	2300
	OVST	24.2	2250
	PULSE	1390.4	2010
4275 GtC	FAST	22	2250
	MEDIUM	17	2300
	SLOW	14.1	2350
	OVST	28.2	2300
	PULSE	1897.2	2010
5275 GtC	FAST	24.9	2300
	MEDIUM	21.1	2350
	SLOW	15.9	2400
	OVST	34.9	2350
	PULSE	2404.1	2010

ESDD
5, 747–778, 2014

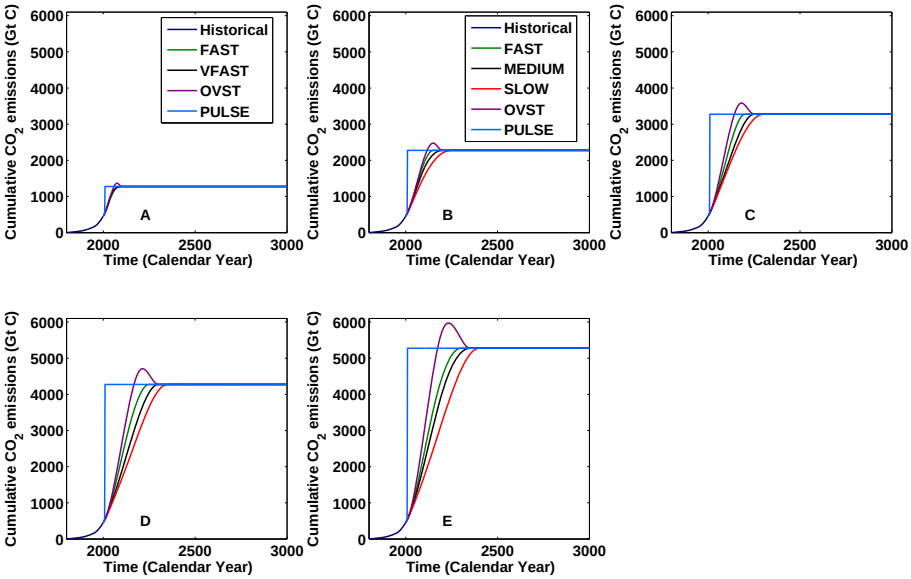

Figure 1. Global cumulative CO_2 emissions (fossil fuel plus LUC emissions) for the 1275–5275 GtC cumulative emission scenarios. **(a)** 1275 GtC scenarios, **(b)** 2275 GtC scenarios, **(c)** 3275 GtC scenarios, **(d)** 4275 GtC scenarios, and **(e)** 5275 GtC scenarios. (Note: legend for **(b)** also applies to **(c–e)**.)

ESDD
5, 747–778, 2014

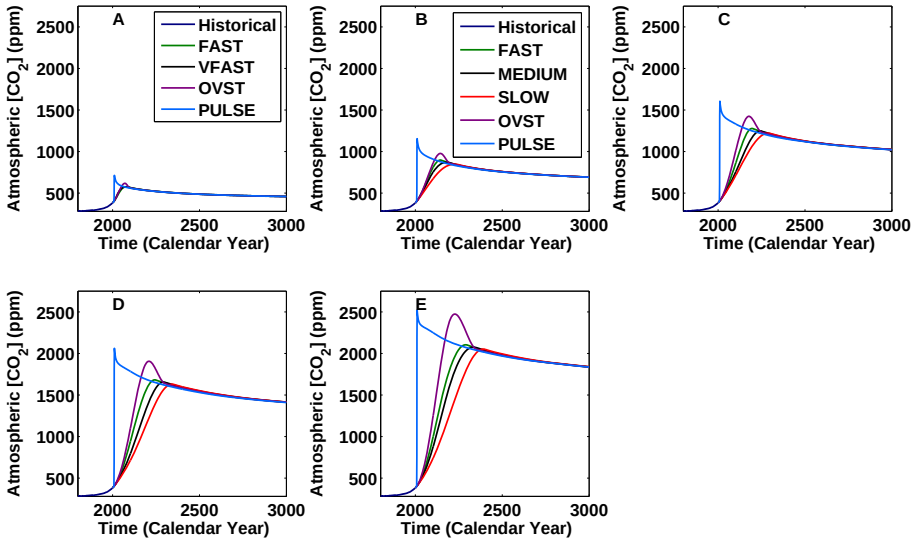

Figure 2. Atmospheric CO_2 concentration for the 1275–5275 GtC scenarios. **(a)** 1275 GtC scenarios, **(b)** 2275 GtC scenarios, **(c)** 3275 GtC scenarios, **(d)** 4275 GtC scenarios, and **(e)** 5275 GtC scenarios. (Note: legend for **(b)** also applies to **(c–e)**.)

ESDD
5, 747–778, 2014

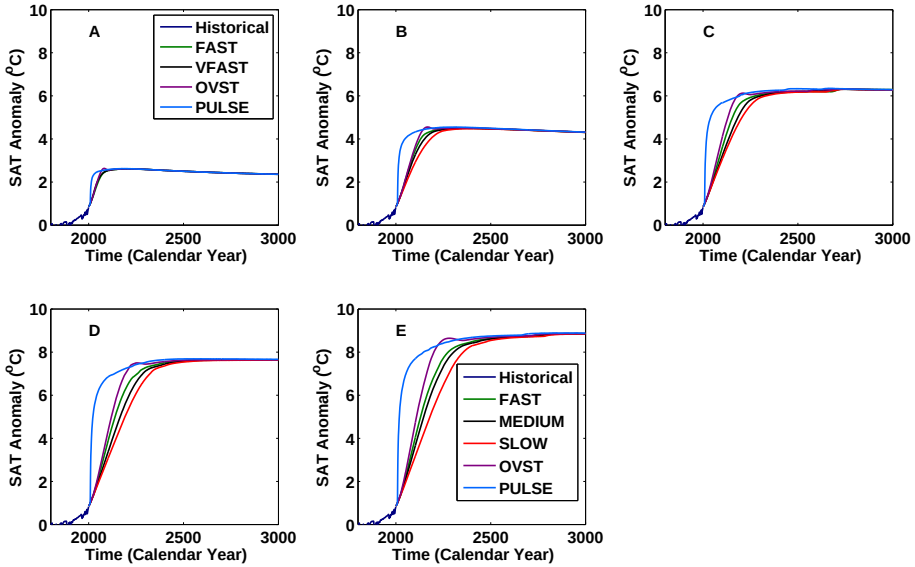

Figure 3. Global mean surface air temperature (SAT) anomaly relative to the year 1800 for the 1275–5275 GtC scenarios. **(a)** 1275 GtC scenarios, **(b)** 2275 GtC scenarios, **(c)** 3275 GtC scenarios, **(d)** 4275 GtC scenarios, and **(e)** 5275 GtC scenarios. (Note: legend for **(e)** also applies to **(b–d)**.)

ESDD
5, 747–778, 2014

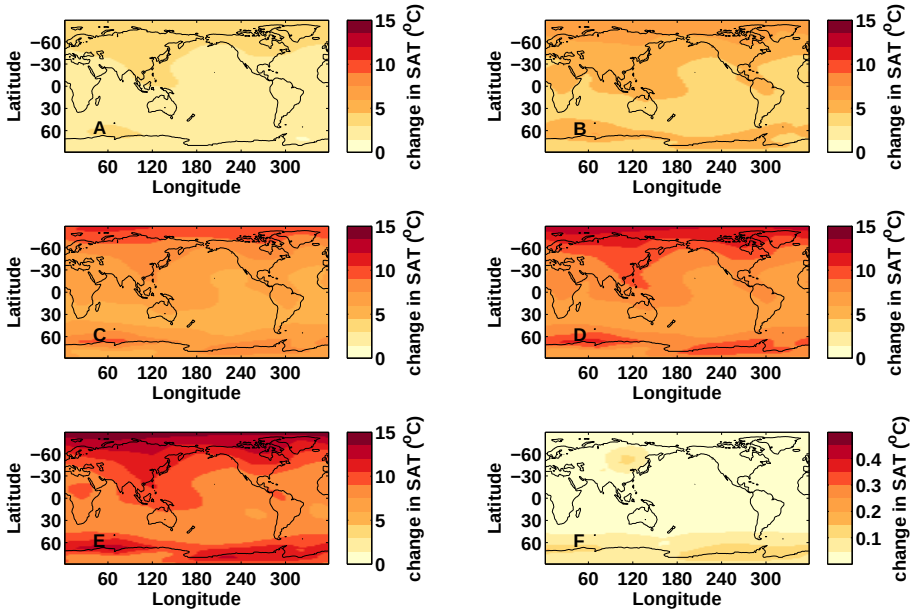

Figure 4. Year 3000 surface air temperature (SAT) anomalies relative to 1800 for select scenarios. **(a)** 1275 GtC FAST, **(b)** 2275 GtC FAST, **(c)** 3275 GtC FAST, **(d)** 4275 GtC FAST, **(e)** 5275 GtC FAST, and **(f)** 5275 GtC PULSE minus SLOW. Note that the color scale for **(f)** is different from that for the other panels.

ESDD
5, 747–778, 2014

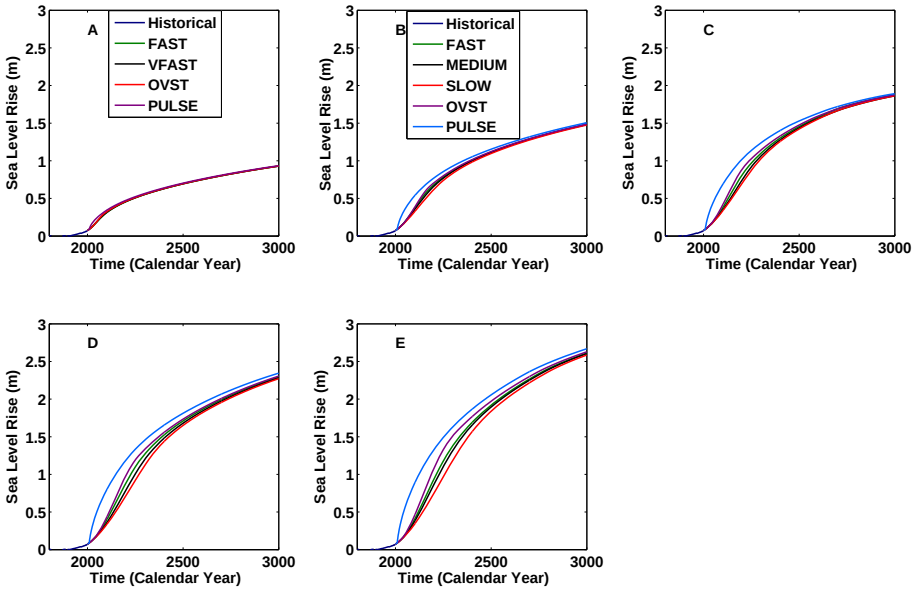

Figure 5. Global mean thermosteric sea level rise (relative to 1800) for the 1275–5275 GtC scenarios. **(a)** 1275 GtC scenarios, **(b)** 2275 GtC scenarios, **(c)** 3275 GtC scenarios, **(d)** 4275 GtC scenarios, and **(e)** 5275 GtC scenarios. (Note: legend for **(b)** also applies to **(c–e)**.)

ESDD
5, 747–778, 2014

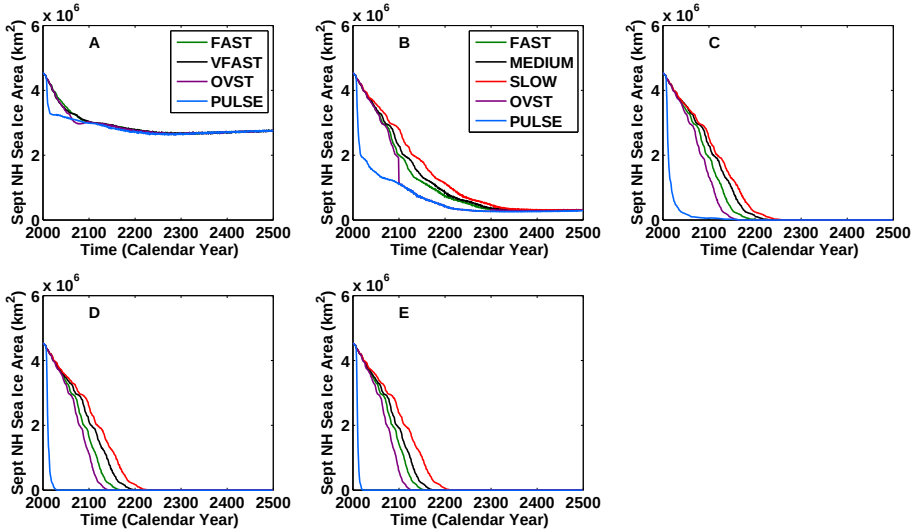

Figure 6. September Northern Hemisphere (NH) sea ice area (km^2) for the 1275–5275 GtC scenarios. **(a)** 1275 GtC scenarios, **(b)** 2275 GtC scenarios, **(c)** 3275 GtC scenarios, **(d)** 4275 GtC scenarios, and **(e)** 5275 GtC scenarios. (Note: legend for **(b)** also applies to **(c–e)**.)

ESDD
5, 747–778, 2014

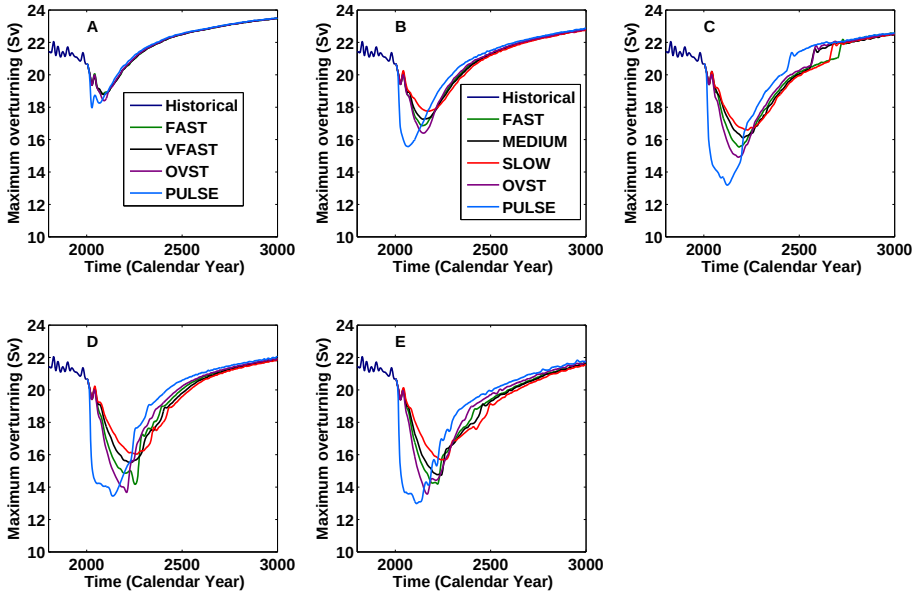

Figure 7. Atlantic Meridional Overturning Circulation (AMOC) index (defined as the maximum overturning streamfunction) for the 1275–5275 GtC scenarios. **(a)** 1275 GtC scenarios, **(b)** 2275 GtC scenarios, **(c)** 3275 GtC scenarios, **(d)** 4275 GtC scenarios, and **(e)** 5275 GtC scenarios. (Note: legend for **(b)** also applies to **(c–e)**.)

ESDD
5, 747–778, 2014

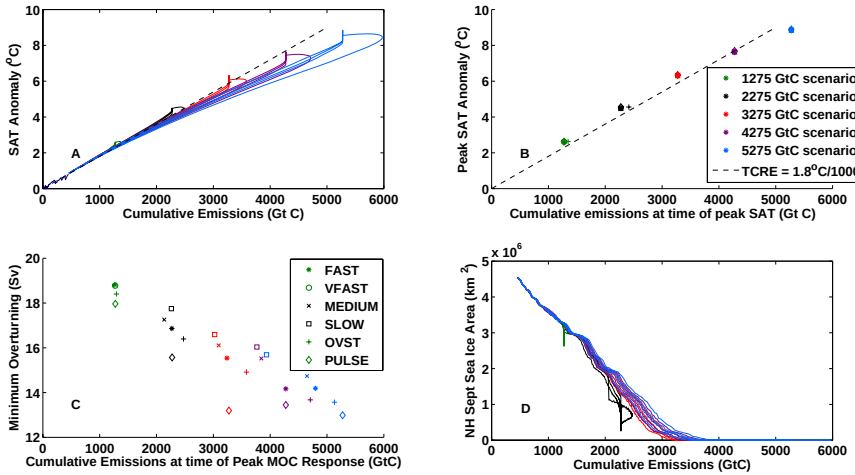

Figure 8. Relationship between physical climate variables and cumulative carbon emissions. **(a)** Global mean surface air temperature (SAT) anomaly (relative to 1800), **(b)** peak global mean surface air temperature anomaly (relative to 1800), **(c)** minimum overturning circulation, and **(d)** September Northern Hemisphere (NH) sea ice area. The dashed line in **(a)** and **(b)** shows the relationship between SAT change and cumulative emissions using the average TCRE computed at the time of CO_2 doubling ($1.8\,^{\circ}\mathrm{C}\,\mathrm{TtC}^{-1}$). Note: the colour legend in **(b)** applies to all panels and the symbol legend in **(c)** applies to **(b)** and **(c)**.

ESDD
5, 747–778, 2014

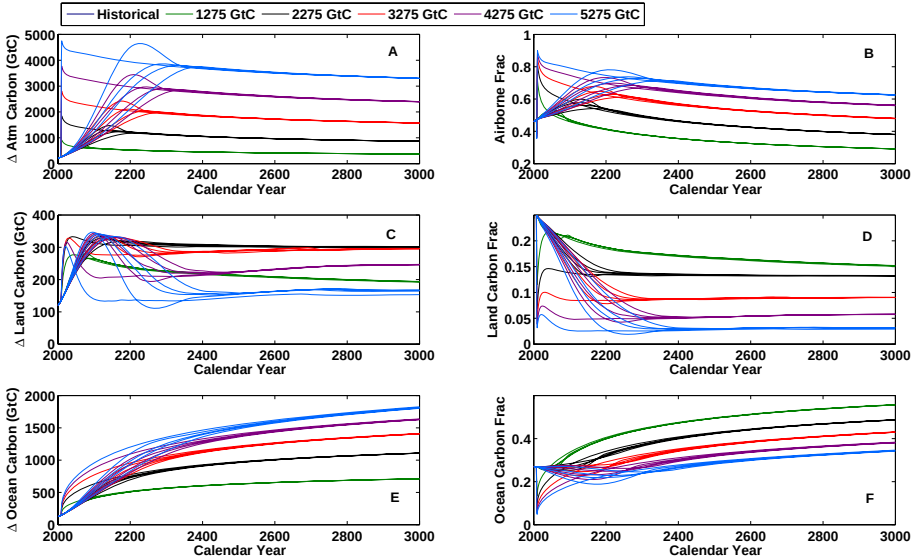

Figure 9. Global carbon cycle response. **(a)** Atmospheric carbon anomaly (w.r.t. 1800), **(b)** airborne fraction of cumulative emissions, **(c)** land carbon anomaly (w.r.t. 1800), **(d)** fraction of cumulative emissions taken up by the land, **(e)** ocean carbon anomaly (w.r.t. 1800), **(f)** ocean uptake fraction. Note that vertical axes vary.

ESDD
5, 747–778, 2014

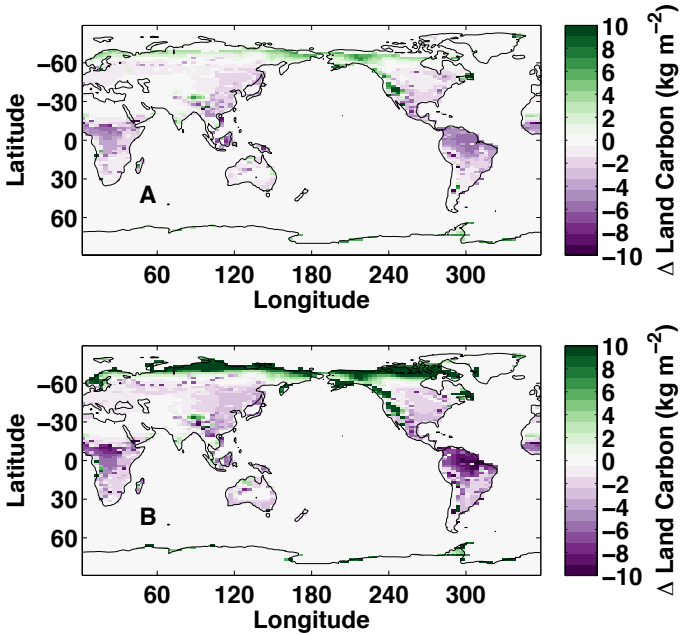

Figure 10. Changes in land carbon for the 5275 GtC FAST scenario. **(a)** Minimum (year 2310) minus peak (year 2170) total land carbon, **(b)** year 2990 minus minumum (year 2310) total land carbon.

ESDD
5, 747–778, 2014